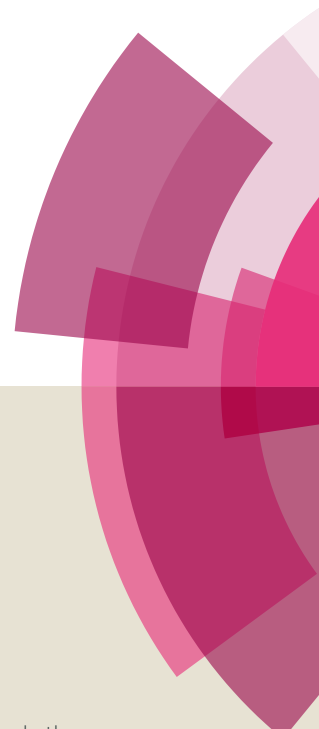


NJC

Accepted Manuscript



This article can be cited before page numbers have been issued, to do this please use: S. L. Jain, A. Kumar and A. Sundaram, *New J. Chem.*, 2019, DOI: 10.1039/C9NJ00852G.



This is an Accepted Manuscript, which has been through the Royal Society of Chemistry peer review process and has been accepted for publication.

Accepted Manuscripts are published online shortly after acceptance, before technical editing, formatting and proof reading. Using this free service, authors can make their results available to the community, in citable form, before we publish the edited article. We will replace this Accepted Manuscript with the edited and formatted Advance Article as soon as it is available.

You can find more information about Accepted Manuscripts in the [author guidelines](#).

Please note that technical editing may introduce minor changes to the text and/or graphics, which may alter content. The journal's standard [Terms & Conditions](#) and the ethical guidelines, outlined in our [author and reviewer resource centre](#), still apply. In no event shall the Royal Society of Chemistry be held responsible for any errors or omissions in this Accepted Manuscript or any consequences arising from the use of any information it contains.

Silver doped reduced graphene oxide as promising plasmonic photocatalyst for oxidative coupling of benzylamines under visible light irradiation

View Article Online
DOI: 10.1039/C9NJ00852GAnurag Kumar,^{1,2} Aathira M. Sadanandhan,¹ and Suman L. Jain^{1*}¹Chemical Sciences Division, CSIR-Indian Institute of Petroleum, Dehradun India 248005²Academy of Scientific and Innovative Research (AcSIR), New Delhi India 110001

Abstract

Visible light assisted photocatalytic transformations have been considered as an efficient and sustainable approach for the production of high-value chemicals. The present paper describes the synthesis of plasmonic silver nanoparticles incorporated reduced graphene oxide and its photocatalytic performance for the selective oxidation of various benzylamines to the corresponding imines using molecular oxygen as oxidant under ambient temperature condition. The developed photocatalyst was found to be highly stable and exhibited excellent photoactivity with consistent recycling ability for several runs without loss in activity. Moreover, to the best of our knowledge, the developed photocatalyst represents the first example of a graphene-based photocatalyst for the oxidative coupling of amines.

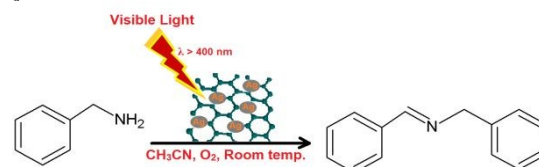
Introduction

Imines and their derivatives have found extensive applications as key intermediates for preparation of various nitrogen containing heterocyclic compounds mainly in alkaloid synthesis.^{1,2} Oxidative coupling of amines is a straight forward approach for the synthesis of these valuable intermediates.³⁻⁸ Furthermore, the use of abundantly available solar energy and molecular oxygen as oxidant make this methodology greener and sustainable.^{6,9-12} However, limited reports mainly using semiconductor-based photocatalysts are known in the previous literature for the oxidation of benzylamines to imines using molecular oxygen as oxidant. Su and co-workers investigated mesoporous graphite carbon nitride (mpg-C₃N₄) for the oxidation of benzylic alcohols and amines with O₂ under visible light.¹³ Jin et al. demonstrated the selective oxidation of amines using O₂ catalyzed by cobalt thioporphyrine under visible light.¹⁴ Raza et al. reported oxidative coupling of amines by photoactive WS₂ nanosheets.¹⁵ Furukawa et al. demonstrated the use of Nb₂O₅ as an efficient heterogeneous photocatalyst for the oxidation of various amines into respective imines in the presence of molecular oxygen as an oxidant.¹⁶ Sun et al. reported visible-light-assisted photocatalytic oxidation of amines to imines over NH₂-MIL-125(Ti) photocatalyst.¹⁷ Very recently Kumar et al. reported a hybrid photocatalyst consisting of iron bipyridine complex immobilized to graphitic carbon nitride under visible light irradiation¹⁸.

Graphene, the newest member of carbon family, possesses two-dimensional layered structure of sp² hybridized carbon atoms and unique properties that are useful in catalysis and photovoltaic devices.¹⁹ Due to the abundance of delocalized electrons from the conjugated sp² bonded carbon network, graphitic carbon enhances the transport of photo-generated electrons and increases the photo-conversion efficiency of the system.²⁰⁻²⁵ Although, graphene oxide (GO)/ reduced graphene oxide (rGO) owing to their lower bandgap have been used as visible light active semiconductor photocatalyst, albeit the conversions were found to be poor due to fast recombination of electron-hole pairs on the surface²⁴⁻²⁶. In order to enhance the photo-conversion efficiency of GO/rGO based photocatalysts by suppressing the electron-hole recombination, surface modifications with noble metal ions, such as platinum, palladium, silver and gold nanoparticles (NPs) has been well established.²⁷⁻³² Among the most studied noble metals, silver owing to its low cost, unique optical properties, higher chemical stability and non-toxic nature has considered to be promising for the modifications of graphene and its analogs for photocatalytic

applications.³³⁻³⁵ Further immobilization of silver nanoparticles on reduced graphene oxide is known to improve the performance mainly due to the increased reactive surface area, as well as the superior charge separation. The unique electron collecting and transporting properties of graphene through conjugated system drive the hot electrons to the reactive sites, and suppressing the recombination. Owing to these advantages we have chosen Ag@rGO photocatalyst for the present study.

Accordingly, we herein report the synthesis, characterization and performance evaluation of the silver NPs decorated reduced graphene oxide, i.e. Ag@rGO for the oxidative coupling of benzylamines with molecular oxygen under ambient conditions using visible light irradiation (Scheme 1). To the best of our knowledge the present study represents the first report on the use of graphene-based photocatalyst for oxidative coupling of benzylamines.

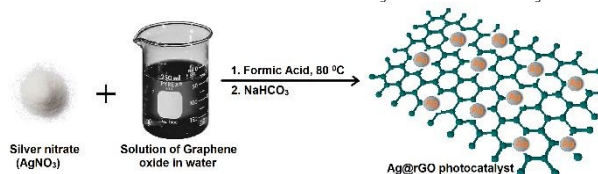


Scheme 1: Oxidative coupling of benzylamines under visible light.

Results and discussion

Synthesis and characterization of the photocatalyst

The desired photocatalyst (Ag@rGO) was obtained by in-situ synthesis of silver nanoparticles (Ag NPs) followed by reduction of graphene oxide into rGO in the presence of formic acid at 80 °C as shown in Scheme 2. Loading of Ag NPs in photocatalyst was found to be 5 wt% as determined by ICP-AES analysis.



Scheme 2: Synthesis of Ag@rGO photocatalyst

The surface morphology of the photocatalyst was determined by HR-TEM analysis. The HR-TEM images showed in Fig. 1a-b revealed the wrinkled nanosheets like morphology with encapsulation of Ag NPs in rGO nanosheets. Fig. 1c-d showed lattice spacing around 0.235 nm corresponded to (111) plane of Ag NPs according to the JCPDS No. 04-0783.³⁶ The average particle size of the Ag NPs obtained from the HR-TEM image was approximately in the range of 10-12 nm. The SAED pattern showed that the synthesized material was crystalline in nature. The elemental mapping confirmed the homogeneous dispersion of the Ag NPs throughout the material (Fig. S1). Furthermore, the EDX (Fig. S1) confirmed the presence of all the desired elements i.e. C, O and Ag in the hybrid material.

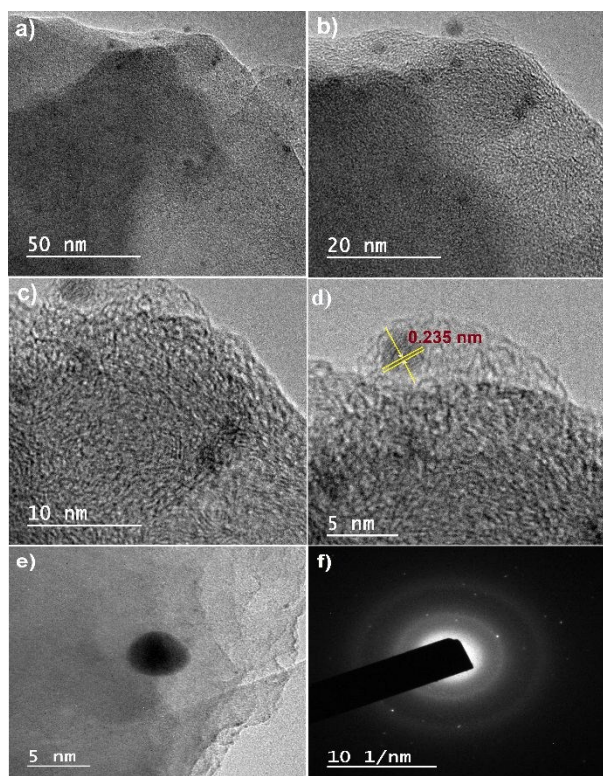


Fig. 1 HR-TEM images: a) Ag@rGO; b) at 20 nm showing the presence of Ag NPs; c) at 10 nm show the fringes d) 5 nm scale bar showing interplanar d-spacing; f) SAED pattern.

Fig. 2 demonstrates the FTIR spectra of GO, rGO and Ag@rGO photocatalyst. FTIR spectrum of GO showed the characteristic bands related to -OH (3000-3500 cm^{-1}), C-H ($\nu_{\text{C-H}}$ at 2923 cm^{-1}), C=C ($\nu_{\text{C=C}}$ at 1574 cm^{-1}), C-OH ($\nu_{\text{C-OH}}$ at 1383 cm^{-1}), C-O-C ($\nu_{\text{C-O-C}}$ at 1249 cm^{-1}), C-O ($\nu_{\text{C-O}}$ at 1055 cm^{-1}) and C=O ($\nu_{\text{C=O}}$ at 1725 cm^{-1}) of the oxygen functionalities present on the basal plane of graphene sheets (Fig. 2a).^{37,38} FTIR spectrum of rGO showed the reduced intensity of all the bands related to the oxygen functionalities and exhibited mainly two absorption bands at 1249 cm^{-1} ($\nu_{\text{C-O-C}}$) and 1574 cm^{-1} ($\nu_{\text{C=C}}$), which indicated the successful reduction of the GO to rGO (Fig. 2b). After the intercalation of Ag NPs between the graphitic sheets of rGO or deposition onto the surface of nanosheets, the FTIR spectrum of hybrid remains almost similar to rGO with reduced intensity of the bands. The bands at 3411 cm^{-1} (OH), 1574 cm^{-1} (C=C) and 1249 cm^{-1} (C-O-C) could be clearly seen in the FTIR spectrum of the photocatalyst with slightly reduced intensity (Fig. 2c).

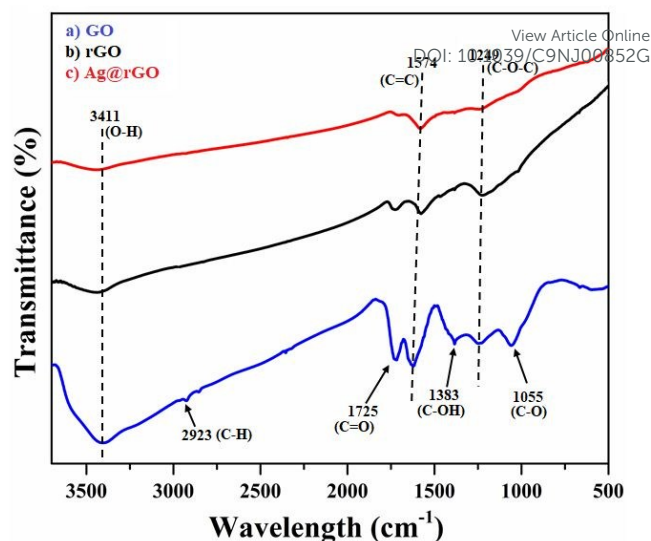


Fig. 2 FTIR Spectra of a) GO, b) rGO, c) Ag@rGO

The crystalline nature and phase structure of the synthesized samples was determined by XRD analysis (Fig. 3). The diffractogram of GO showed a sharp peak at $2\theta=10.27^\circ$ corresponded to (001) plane (Fig. 3a).³⁹ In case of rGO an intense broad peak at 25.4° and a small peak at 43.6° corresponding to (002) and (111) planes, respectively were appeared (Fig. 3b).⁴⁰ In hybrid Ag@rGO photocatalyst, the peaks observed at 38.1° , 44.3° , 64.5° and 77.3° were corresponded to (111), (200), (220) and (311) crystallographic planes of Ag NP phase. The average particle size in the photocatalyst was estimated by using the Debye-Scherrer formula.

$$D = 0.9\lambda / \beta \cos\theta \dots\dots\dots(1)$$

where " λ " is wavelength of X-ray (1.5418 Å), " β " is FWHM (full width at half maximum), " θ " is the diffraction angle and " D " is particle diameter size. The average particle size of Ag NPs was found to be in the range of 12 nm. The peak at 25.4° indexed to (002) planes with 0.235 nm interlayer distance is attributed to the presence of graphene in the hybrid material (Fig. 3c).⁴¹ The average estimated crystallite size of the Ag NPs at optimum condition was found to be in the range of 8-10 nm that matches well with the sizes of Ag NPs obtained from HR-TEM analysis.

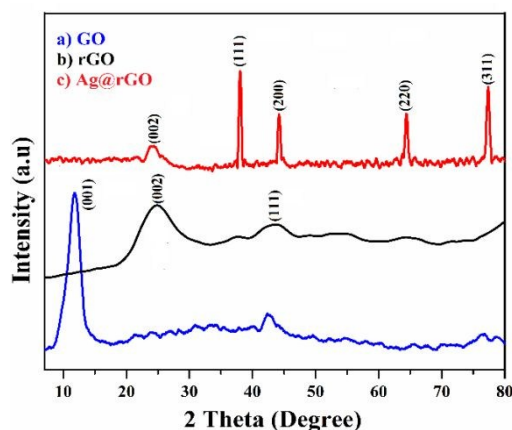


Fig. 3 XRD pattern of a) GO, b) rGO, c) Ag@rGO photocatalyst.

Fig. 4 shows the Raman spectra of the reduced graphene oxide and Ag@rGO hybrid material. In case of rGO two bands, i.e., D band and G band at 1335 and 1594 cm^{-1} respectively are obtained (Fig. 4a). The intensity ratio of D to G defines the degree of distortion in the graphitic sheets. The integral intensity ratio of D to G bands (ID/IG) in rGO was found to be 0.97. After intercalation of the Ag NPs, the integral intensity ratio ID/IG was found to be increased, i.e. 1.18, which suggested the presence of a large number of defects in the form of Ag NPs in the hybrid (Fig. 4b).⁴²

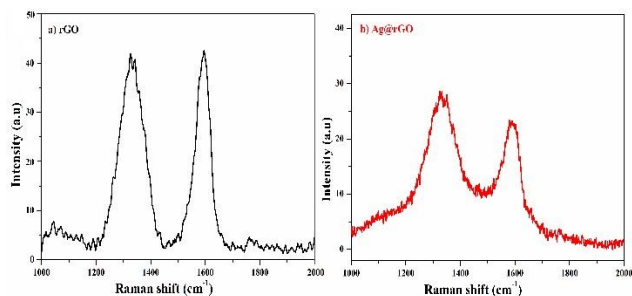


Fig. 4: Raman spectra of a) rGO, b) Ag@rGO photocatalyst.

UV-Vis spectroscopy was used to determine the absorbance of GO, rGO, and Ag@rGO photocatalysts. In case of GO, the absorbance in the region between 250-280 nm owing to the $\pi-\pi^*$ transitions of aromatic C-C bonds indicated the restoration of the extensive conjugated framework of sp^2 carbons and a shoulder at about 300 nm assigned to $n-\pi^*$ transition of C=O bonds (Fig. 5a). For rGO the absorption peak corresponds to $\pi-\pi^*$ transition of the aromatic C-C bond was found to be redshifted to 270 nm, confirmed the reduction of GO (Fig. 5b). UV-Vis spectrum of Ag@rGO hybrid exhibited strong absorption in the visible region 350-370 nm due to the surface plasmonic resonance (SPR) of Ag NPs, which further confirmed its application as a visible light active photocatalyst for organic transformations (Fig. 5c).⁴³ Furthermore, the band gap observed for rGO and Ag@rGO hybrid was 1.72 and 1.5 eV, respectively as calculated with the help of a Tauc plot with linear extrapolation (Fig. S2). The rate of charge recombination was analyzed with the help of Photoluminescence spectroscopy. The PL spectra of rGO displayed a peak at 478 nm with high intensity. However, the significant lowering in peak intensity in hybrid photocatalyst confirmed the reduced charge recombination (Fig. S3).

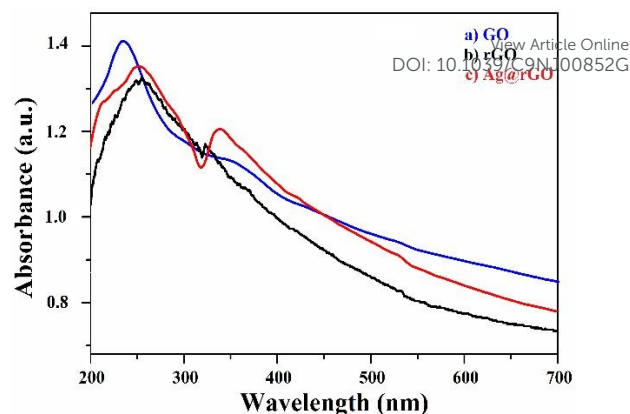


Fig. 5: UV-vis absorption spectra of a) GO, b) rGO, c) Ag@rGO photocatalyst.

X-ray photoelectron spectroscopy was used to determine the surface chemical composition of the photocatalyst. The XPS survey scan shows the binding energies of all desired elements such as C_{1s} (285.0 eV), O_{1s} (531.5 eV), Ag_{3d} (368 eV) and Ag_{3d} (374 eV) in hybrid material (Fig. 6a). The high-resolution XPS spectra of C_{1s} shows three peaks at ~ 284 , 285.3 and 288.2 eV due to C-C and C-O and C=O bonds, respectively confirmed the presence of reduced graphene oxide (Fig. 6b).⁴⁴ For the comparison, we added the XPS of graphene oxide which exhibited C_{1s} peaks at binding energy 285.8 and 287.9 eV due to the C-C and C-O bond respectively (Fig. 6b). The XPS high-resolution spectrum of O_{1s} deconvoluted into two peaks at 532.3 and 530.8 eV corresponded to O-H and C=O, respectively (Fig. 6c). Fig 6d shows the high-resolution spectrum of Ag_{3d} , in which two peaks appeared at 374 and 368 eV with spin energy separation of 6 eV attributed to $\text{Ag}_{3d_{5/2}}$ and $\text{Ag}_{3d_{3/2}}$, respectively (Fig. 6c). These values confirm that silver is present as Ag^0 in the hybrid photocatalyst. The reduction of Ag^+ to Ag^0 occurred on the surface of rGO sheets during the reduction process.^{45,46}

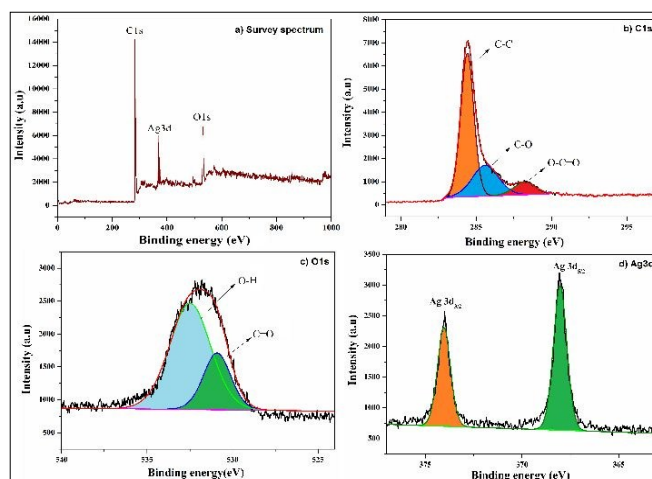


Fig. 6: High-resolution XPS spectra of Ag@rGO photocatalyst.

The thermal stability of the synthesized hybrid was measured by thermo-gravimetric analysis (TGA). Thermogram of Ag@rGO photocatalyst showed an initial weight loss at temperature 100 $^{\circ}\text{C}$ due to the evaporation of moisture and a gradual weight loss in the range of 300-500 $^{\circ}\text{C}$ owing to the combustion of the carbon skeleton of graphene (Fig. S4). The nitrogen adsorption-desorption isotherm for Ag@rGO was of type-IV that confirmed the mesoporous nature of the material. The higher absorption capacity of the photocatalyst could be attributed to the larger surface area of the material. The S_{BET} and pore volume for Ag@rGO were found to be 88.2 m^2g^{-1} and 0.25 cm^3g^{-1}

respectively (Fig. S5).

Photocatalytic oxidative coupling of benzylamines

The photocatalytic activity of the synthesized photocatalyst was evaluated for the oxidative coupling of benzylamines to imines with molecular oxygen under visible luminance at room temperature using acetonitrile as reaction medium (Scheme 1). At first, the oxidative coupling of benzylamine was chosen as a representative reaction for screening experiments. The results of these experiments are summarized in Table 1. To evaluate the effect of loading of Ag NPs in the hybrid photocatalyst, two more samples using different amount of Ag NPs (3 and 7 wt%) was prepared and tested under identical conditions. The activity order of these materials was found to be in the order 3%Ag@rGO < 5%Ag@rGO > 7%Ag@rGO (Table 1, entry 1). The poor product yield in 3% Ag@rGO might be due to the less concentration of the reactive Ag⁰-sites on the surface; whereas leaching of active Ag⁰-content from the surface in 7% Ag@rGO was responsible for the poor reactivity. Hence, 5%Ag@rGO was considered to be optimum photocatalyst for this transformation. Among the different solvents such as DMF, methanol, ethanol, THF and acetonitrile studied, acetonitrile was found to be best for this transformation (Table 1, entry 2). Visible light irradiation was found to be essential and there was no reaction occurred in the dark under described conditions (Table 1, entry 3). Similarly, there was no reaction observed in the absence of photocatalyst under visible irradiation even after the prolonged reaction time (Table 1, entry 3). The use of individual components, such as rGO and Ag NPs as photocatalysts under the identical conditions afforded only 13 and 17% conversion of benzylamine, respectively (Table 1, entry 4-5). Molecular oxygen was found to be vital, and a negligible yield of the desired product was obtained when nitrogen was used in place of oxygen (Table 1, entry 6).

Table 1: Results of screening experiments.^a

Entry	Visible light	Photocatalyst	Solvent	Conv. (%) ^b
1	Yes	5%Ag@rGO	CH ₃ CN	98
		3%Ag@rGO		56
		7%Ag@rGO		84
2	Yes	5%Ag@rGO	DMF	91
			MeOH	72
			THF	54
			EtOH	75
3	No	5%Ag@rGO	CH ₃ CN	-
	Yes	- ^c	-	-
4	Yes	Ag NPs	CH ₃ CN	17
5	Yes	rGO	CH ₃ CN	13
6 ^d	Yes	5%Ag@rGO	CH ₃ CN	-

^aReaction conditions: benzylamine (1 mmol), photocatalyst (25 mg), solvent (10 mL), light source: white cold LED $\lambda > 400$ nm, time: 12h using molecular oxygen as oxidant; ^bdetermined by GC-MS; ^cReaction time, 24h; ^dIn the absence of molecular oxygen (under N₂ atmosphere).

Based on these experiments, it can also be concluded that the main reactive sites for this transformation in the developed photocatalyst were Ag NPs. However supporting them to rGO significantly improved the reactivity and provided higher conversion and product yield. The presence of rGO support in the photocatalyst mainly provided increased surface area, facile collection and transportation of the electrons on the surface to suppress the recombination of electrons and holes, and finally

higher concentration of the substrate on the vicinity of the reactive sites through the π - π interaction. Hence, the presence of rGO support improved the reactivity of the photocatalyst.

The scope of the reaction was extended for various substituted benzylamines under optimized reaction conditions. The results of these experiments are summarized in Table 2. As shown in Table 2, all the reactants containing either electron donating or withdrawing groups were selectively and efficiently converted to the corresponding *N*-benzylidene benzylamines with excellent yields without any evidence of the formation of any by-product. Among the various substrates, benzylamines substituted with electron-donating groups i.e. OCH₃, CH₃ (Table 2, entries 2-4) were found to be more reactive as compared to those having electron withdrawing groups, i.e. Cl, F, Br (Table 2 entries 6-9). The higher reactivity of the electron-rich substrates may be assumed due to the facile formation of cation radical followed by imine intermediate after donating electron to VB of the photocatalyst during the reaction. Substrates like aniline, cyclohexylamine and *n*-butyl amine did not show any reaction under the described protocol, and original substrates could be isolated at the end of the reaction (Table 1, entry 10-12).

Table 2: Ag@rGO catalyzed oxidative coupling of amines under visible light irradiation.

Entry	Reactants	Products	Conv. (%) ^b	Yield (%) ^c	TOF (h ⁻¹)
1			98	97	8.0
2			96.5	94	7.8
3			93	91	7.5
4			88	87	7.2
5			85	83	6.9
6			83	82	6.8
7			86	84	7.0
8			89	87	7.2
9			84	82	6.8
10		-	-	-	-
11		-	-	-	-
12		-	-	-	-

^aReaction conditions: substrate (1 mmol), 5%Ag@rGO (25 mg), acetonitrile (10 mL) under visible light irradiation with white cold LED $\lambda > 400$ nm; time: 12 h using molecular oxygen as oxidant; Power at reaction vessel: 70 W/m²; ^bdetermined by GC-MS; ^cIsolated yield.

Further, the recyclability experiments were performed by selecting the oxidative coupling of benzylamine as a representative example. After completion of the reaction, the photocatalyst was easily separated by filtration, washed with acetonitrile, dried and reused for subsequent experiment with fresh substrate. The results of recycling experiments are depicted in Fig. 7. The conversion and product yield remained almost same for seven cycles, confirming that the developed catalyst was highly stable and reusable with consistent efficiency. Further to check the leaching of Ag NPs during the reaction, selected filtrate samples were analyzed by ICP-AES analysis.

There was no detectable amount of Ag NPs observed, which eliminated the possibility of leaching of Ag during the photoreactions. Furthermore, the metal loading in the recovered photocatalyst after 7th run was found to be 4.98 wt% which was almost similar to the fresh one (5 wt%). These results indicated that the developed photocatalyst was highly stable, heterogeneous and no leaching had occurred during the photocatalytic experiments.

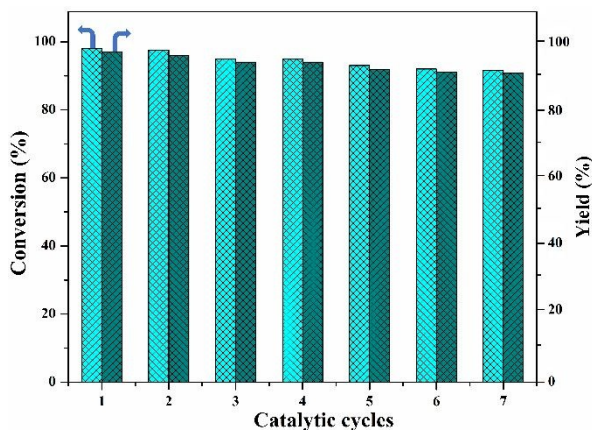
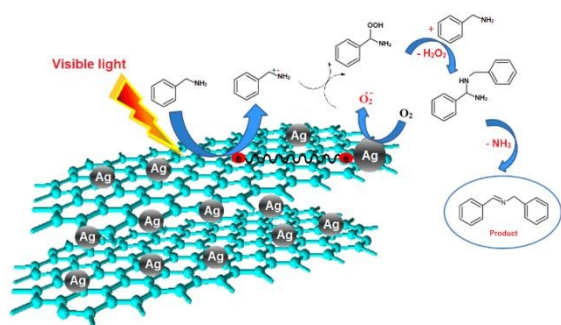


Fig. 7: Results of recycling experiments

The exact mechanism of the reaction is not known at this stage. Based on the existing reports, a plausible mechanism of the reaction is proposed as shown in Scheme 2. Under the light irradiation, charge separation takes place in the photocatalyst and photo-generated electrons are produced in the conduction band (CB) and photo-generated holes remain in the valence band (VB). The presence of rGO owing to its 2D planar conjugated structure facilitated the charge separation and provided mobility of these electrons on the photocatalyst surface.⁴⁷ These hot electrons react with oxygen molecules adsorbed on the rGO surface and converted to $O_2^{\cdot-}$ radicals.⁴⁸ These $O_2^{\cdot-}$ radicals are very powerful oxidizing agents and can oxidize benzylamine to imine under visible-light irradiation. At the same time, reactive holes in the VB of Ag are able to oxidize benzylamine molecule directly due to their strong oxidizing ability. As a result, the separated electrons and holes are fully involved in the photocatalytic reactions and provided improved activity.



Scheme 2: Plausible mechanism of photocatalytic oxidative coupling of benzylamine in the presence of Ag@rGO photocatalyst.

Furthermore, in order to verify the suggested mechanism we performed the quenching experiments by using NaN_3 as quencher. A comparison between the original photocatalytic experiment and that obtained after the addition of sodium azide (NaN_3) at different time intervals followed by the analysis by GC-MS (Fig. 8) was made to visualize the quenching effect of azide ions. After adding NaN_3 as quencher the maximum conversion of benzylamine in the presence of hybrid photocatalyst was reached only up to 13.7% after 12h. While in case of original photocatalytic experiment, the maximum

conversion reached up to 98% under same reaction conditions. These experimental results confirmed the generation of singlet oxygen (1O_2) in the photocatalytic system under visible light irradiation.

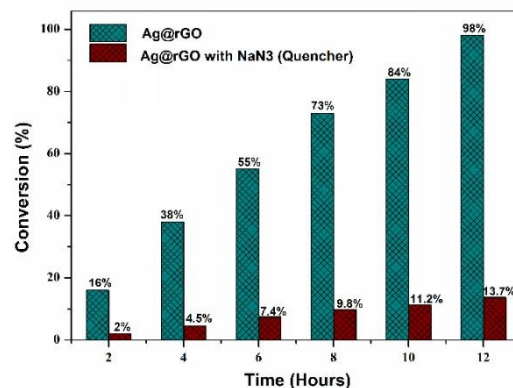


Fig. 8: Conversion of benzylamine using Ag@rGO photocatalyst as such and with adding NaN_3 as a quencher.

Conclusions

We have demonstrated an efficient, easily synthesized and cost-effective heterogeneous photocatalyst prepared by single step in-situ grafting of the Ag NPs onto the surface of rGO for the oxidative coupling of benzylamines to imines under visible light at room temperature. The developed photocatalyst exhibited higher efficiency as compared to its individual components such as rGO and Ag NPs and reported photocatalysts in the prior art (Table S1). More importantly, the photocatalyst showed consistent recycling for several runs without any remarkable loss of the activity. This study promotes the synthesis of graphene-based heterogeneous materials for visible light assisted organic transformations.

Experimental

Materials

All chemicals were analytical reagent grade and used as received without further purification. Graphite flakes, potassium permanganate (99%), sodium nitrate (99%), silver nitrate ($AgNO_3$), sodium borohydride ($NaBH_4$) was purchased from Sigma-Aldrich. Hydrogen peroxide (30%), acetonitrile, formic acid, hydrochloric acid and sulphuric acid (H_2SO_4) procured from Alfa Aesar. The deionized (DI) water used throughout the experiments was of HPLC grade. Graphene oxide was synthesized from graphite powder according to the modified method reported by Hummers and Offeman⁴⁹.

Synthesis of in situ Ag@rGO hybrid photocatalyst⁵⁰

Graphene oxide (1.0 g) was sonicated with 50 ml DI water, and then 2 mL of formic acid was mixed in the reaction mixture. Subsequently, $AgNO_3$ (50 mg) was added as a precursor of Ag NPs in the hybrid material. The reaction mixture was heated at 80 °C for 6 h under continuous stirring. The solid was separated by filtration and washed with deionized water for several times followed by a saturated solution of sodium bicarbonate to remove the excess formic acid. Finally the solid was washed with deionized water and dried under vacuum for overnight at 60 °C for 6h. For the comparative study, bare reduced graphene oxide (rGO) was prepared by following the similar procedure without adding silver nitrate. Similarly, other Ag@rGO samples containing different amount of Ag NPs were prepared for the comparative study.

Characterization Techniques

CREATED USING THE RSC ARTICLE TEMPLATE - SEE WWW.RSC.ORG/ELECTRONICFILES FOR FURTHER DETAILS

Surface morphology of the samples was determined by High-resolution transmission electron microscopy (HR-TEM) with JEM 2100, Japan operated at an accelerating voltage of 200 kV using lanthanum hexaboride as a source of electrons. X-ray photoelectron spectroscopy (XPS) measurement of photocatalyst was carried out using ESCA+ (omicron nanotechnology, Oxford instruments Germany) XPS system having an angle between analyzer to the source is 90°. All the binding energies were referenced to the C1s peak at 284.6 eV of the surface adventitious carbon. Fourier Transform Infrared (FT-IR) spectra were recorded on Perkin-Elmer spectrum RX-1 IR spectrophotometer using potassium bromide window. The crystalline structure of the samples was determined by Bruker D8 Advance diffractometer with Cu K α radiation, (λ = 1.5418 Å) in the range of 2θ = 20-80 and a scan rate of 40 min⁻¹. UV-visible spectra of the samples were collected on Perkin Elmer Lambda-19 UV-VIS-NIR spectrophotometer using a 10 mm quartz cell while absorption spectra of solid samples were recorded by using fine powder of BaSO₄ as a reflectance standard. Raman spectra of samples were measured at room temperature using a Raman Microprobe (HR-800 Jobin-Yvon) with 532 nm Nd-YAG excitation source. The specific surface area of the samples was determined by nitrogen adsorption-desorption isotherm at 77 K by using VP; Micromeritics ASAP2010. Thermal degradation pattern of the materials was calculated by TG-DTA analysis by using a thermal analyzer TA-SDT Q-600 in the temperature range of 40 to 800 °C under nitrogen flow with a heating rate 10 °C/min. 1H NMR of the reaction products was collected at 500 MHz by using a Bruker Advance-II 500 MHz instrument.

Acknowledgments

Authors are grateful to Director IIP for granting permission to publish these results. AK express their sincere thanks to CSIR, New Delhi, for providing financial assistance in terms of research fellowship. DST, New Delhi is kindly acknowledged for funding under the project GAP-3125. The analytical division is acknowledged for providing support in the analysis of the samples

References

1. A. V. Kell'in, A. W. Sromek and V. Gevorgyan, *Journal of the American Chemical Society*, 2001, 123, 2074-2075.
2. R. D. Patil and S. Adimurthy, *Asian Journal of Organic Chemistry*, 2013, 2, 726-744.
3. Z. J. Wang, K. Garth, S. Ghasimi, K. Landfester and K. A. Zhang, *ChemSusChem*, 2015, 8, 3459-3464.
4. S. Kegnaes, J. Mielby, U. V. Mentzel, C. H. Christensen and A. Riisager, *Green Chemistry*, 2010, 12, 1437-1441.
5. A. Dhakshinamoorthy, M. Alvaro and H. Garcia, *ChemCatChem*, 2010, 2, 1438-1443.
6. N. Li, X. Lang, W. Ma, H. Ji, C. Chen and J. Zhao, *Chemical Communications*, 2013, 49, 5034-5036.
7. J. Jin, H.-W. Shin, J. H. Park, J. H. Park, E. Kim, T. K. Ahn, D. H. Ryu and S. U. Son, *Organometallics*, 2013, 32, 3954-3959.
8. S. Zavahir and H. Zhu, *Molecules*, 2015, 20, 1941-1954.
9. X. Lang, H. Ji, C. Chen, W. Ma and J. Zhao, *Angewandte Chemie International Edition*, 2011, 50, 3934-3937.
10. A. Kumar, A. Hamdi, Y. Coffinier, A. Addad, P. Roussel, R. Boukherroub and S. L. Jain, *Journal of Photochemistry and Photobiology A: Chemistry*, 2018, 356, 457-463.
11. J. H. Park, K. C. Ko, E. Kim, N. Park, J. H. Ko, D. H. Ryu, T. K. Ahn, J. Y. Lee and S. U. Son, *Organic letters*, 2012, 14, 5502-5505.
12. S. Zhao, C. Liu, Y. Guo, J.-C. Xiao and Q.-Y. Chen, *The Journal of organic chemistry*, 2014, 79, 8926-8931.
13. F. Su, S. C. Mathew, L. Möhlmann, M. Antonietti, X. Wang and S. Blechert, *Angewandte Chemie*, 2011, 123, 683-686.
14. J. Jin, C. Yang, B. Zhang and K. Deng, *Journal of Catalysis*, 2018, 361, 33-39.
15. F. Raza, J. H. Park, H.-R. Lee, H.-I. Kim, S.-J. Jeon and J.-H. Kim, *ACS Catalysis*, 2016, 6, 2754-2759.
16. S. Furukawa, Y. Ohno, T. Shishido, K. Teramura and T. Tanaka, *ACS Catalysis*, 2011, 1, 1150-1153.
17. D. Sun, L. Ye and Z. Li, *Applied Catalysis B: Environmental*, 2015, 164, 428-432.
18. A. Kumar, P. Kumar, C. Joshi, S. Ponnada, A. K. Pathak, A. Ali, B. Sreedhar and S. L. Jain, *Green Chemistry*, 2016, 18, 2514-2521.
19. S. P. Lonkar and A. A. Abdala, *J Thermodyn Catal*, 2014, 5, 1000132.
20. A. Al-Nafiey, A. Kumar, M. Kumar, A. Addad, B. Sieber, S. Szunerits, R. Boukherroub and S. L. Jain, *Journal of Photochemistry and Photobiology A: Chemistry*, 2017, 336, 198-207.
21. A. Kumar, M. Aathira, U. Pal and S. L. Jain, *ChemCatChem*, 2018, 10, 1844-1852.
22. M.-Q. Yang and Y.-J. Xu, *Physical Chemistry Chemical Physics*, 2013, 15, 19102-19118.
23. N. Zhang, Y. Zhang, M.-Q. Yang and Y.-J. Xu, *Current Organic Chemistry*, 2013, 17, 2503-2515.
24. S. Li, T. Zhu, L. Dong and M. Dong, *New Journal of Chemistry*, 2018, 42, 17644-17651.
25. R. Suresh, R. Udayabhaskar, C. Sandoval, E. Ramirez, R. Mangalaraja, H. D. Mansilla, D. Contreras and J. Yáñez, *New Journal of Chemistry*, 2018, 42, 8485-8493.
26. X. Li, R. Shen, S. Ma, X. Chen and J. Xie, *Applied Surface Science*, 2018, 430, 53-107.
27. B. Li, X. Zhang, P. Chen, X. Li, L. Wang, C. Zhang, W. Zheng and Y. Liu, *RSC Advances*, 2014, 4, 2404-2408.
28. S. Min and G. Lu, *The Journal of Physical Chemistry C*, 2011, 115, 13938-13945.
29. M. Zhu, P. Chen and M. Liu, *Acs Nano*, 2011, 5, 4529-4536.
30. X. Meng and Z. Zhang, *Applied Catalysis B: Environmental*, 2017, 209, 383-393.
31. N. Zhang, M.-Q. Yang, Z.-R. Tang and Y.-J. Xu, *ACS nano*, 2013, 8, 623-633.
32. K.-Q. Lu, X. Xin, N. Zhang, Z.-R. Tang and Y.-J. Xu, *Journal of Materials Chemistry A*, 2018, 6, 4590-4604.
33. N. Zhang, M.-Q. Yang, S. Liu, Y. Sun and Y.-J. Xu, *Chemical reviews*, 2015, 115, 10307-10377.
34. C. Han, N. Zhang and Y.-J. Xu, *Nano Today*, 2016, 11, 351-372.
35. H. Yu, P. Xiao, J. Tian, F. Wang and J. Yu, *ACS applied materials & interfaces*, 2016, 8, 29470-29477.
36. K.-C. Hsu and D.-H. Chen, *Nanoscale research letters*, 2014, 9, 193.
37. P. Kumar, A. Kumar, B. Sreedhar, B. Sain, S. S. Ray and S. L. Jain, *Chemistry—A European Journal*, 2014, 20, 6154-6161.
38. K. Samanta, S. Some, Y. Kim, Y. Yoon, M. Min, S.

- 1
2 M. Lee, Y. Park and H. Lee, *Chemical*
3 *Communications*, 2013, 49, 8991-8993.
- 4 39. Q. Du, M. Zheng, L. Zhang, Y. Wang, J. Chen, L.
5 Xue, W. Dai, G. Ji and J. Cao, *Electrochimica Acta*,
6 2010, 55, 3897-3903.
- 7 40. R. K. Gautam, H. Bhattacharjee, S. V. Mohan and A.
8 Verma, *RSC Advances*, 2016, 6, 110091-110101.
- 9 41. R. Georgekutty, M. K. Seery and S. C. Pillai, *The*
10 *Journal of Physical Chemistry C*, 2008, 112, 13563-
11 13570.
- 12 42. K.-C. Hsu and D.-H. Chen, *Nanoscale research letters*,
13 2014, 9, 484.
- 14 43. I. Roy, D. Rana, G. Sarkar, A. Bhattacharyya, N. R.
15 Saha, S. Mondal, S. Pattanayak, S. Chattopadhyay and
16 D. Chattopadhyay, *RSC Advances*, 2015, 5, 25357-
17 25364.
- 18 44. J. Paredes, S. Villar-Rodil, A. Martínez-Alonso and J.
19 Tascon, *Langmuir*, 2008, 24, 10560-10564.
- 20 45. T. Jiao, H. Guo, Q. Zhang, Q. Peng, Y. Tang, X. Yan
21 and B. Li, *Scientific reports*, 2015, 5, 11873.
- 22 46. H. Sun, K. Xu, G. Lu, H. Lv and Z. Liu, *IEEE*
23 *Transactions on Nanotechnology*, 2014, 13, 789-794.
- 24 47. B. Bajorowicz, J. Reszcyńska, W. Lisowski, T.
25 Klimczuk, M. Winiarski, M. Słoma and A. Zaleska-
26 Medynska, *RSC Advances*, 2015, 5, 91315-91325.
- 27 48. Y. Feng, G. Wang, J. Liao, W. Li, C. Chen, M. Li and
28 Z. Li, *Scientific reports*, 2017, 7, 11622.
- 29 49. W. S. Hummers and R. E. Offeman, *Journal of the*
30 *American Chemical Society*, 1958, 80, 1339-1339.
- 31 50. Y. Yoon, K. Samanta, H. Lee, K. Lee, A. P. Tiwari, J.
32 Lee, J. Yang and H. Lee, *Scientific reports*, 2015, 5,
33 14177.

View Article Online
DOI: 10.1039/C9NJ00852G

CREATED USING THE RSC ARTICLE TEMPLATE - SEE WWW.RSC.ORG/ELECTRONICFILES FOR FURTHER DETAILS

View Article Online
DOI: 10.1039/C9NJ00852G

New Journal of Chemistry Accepted Manuscript

1
2
3
4
5
6
7
8
9
10
11
12
13
14
15
16
17
18
19
20
21
22
23
24
25
26
27
28
29
30
31
32
33
34
35
36
37
38
39
40
41
42
43
44
45
46
47
48
49
50
51
52
53
54
55
56
57
58
59
60